Available online at www.sciencedirect.com
ScienceDirect
Trans. Nonferrous Met. Soc. China 33(2023) 141−156
Transactions of Nonferrous Metals Society of China
www.tnmsc.cn

Effect of electrolyte composition on corrosion behavior and tribological performance of plasma electrolytic oxidized TC4 alloy

Cui-ping YANG[1], Xian-ze MENG[1], Xin-ran LI[1], Zhe-xuan LI[1], Hao-jie YAN[1], Lian-kui WU[1], Fa-he CAO[1,2]

1. School of Materials, Sun Yat-sen University, Shenzhen 518107, China;
2. Southern Marine Science and Engineering Guangdong Laboratory (Zhuhai), Zhuhai 519082, China

Received 30 September 2021; accepted 6 January 2022

Abstract: Four kinds of typical plasma electrolytic oxidation (PEO) coatings were prepared on TC4 alloy to investigate the influence of electrolyte composition on the corrosion behavior and tribological performance of the PEO coatings. The results show that both the corrosion behavior and tribological performance of the PEO coatings are highly dependent on the electrolyte composition. The PEO coating fabricated from the electrolyte containing NaH_2PO_2 exhibits the best corrosion resistance owing to its denser inner layer. The PEO coating prepared from the electrolyte containing $NaAlO_2$ reveals the best tribological performance due to the generation of Al_2O_3. To prepare a PEO coating with satisfying corrosion resistance and wear resistance, a composite PEO coating was fabricated from the electrolyte containing NaH_2PO_2 and $NaAlO_2$.

Key words: Ti6Al4V alloy; plasma electrolytic oxidation; polarization curve; wear

1 Introduction

Due to the low density, high specific strength, and good corrosion resistance [1], Ti6Al4V (TC4) alloy has received extensive attention and has been widely used in the marine environment, including power system, cooling system, sonar system, and pressure shell parts of ships [2]. However, TC4 alloy has poor tribological property and is prone to mechanical degradation during the sliding wear or abrasion process, which limits its further application [3−5].

Till now, several strategies have been explored to improve the tribological properties of TC4 alloy, such as physical vapor deposition (PVD) [6], plasma spraying [7], laser surface modification [8], ion implantation [9], and plasma electrolytic oxidation (PEO) [10,11]. Among them, PEO has received great attention in recent years owing to its convenient operation, and good performance of the prepared coating [12,13].

At the initial stage of PEO, the alloy undergoes anodization. With the prolonging of electrolysis, the voltage reaches a critical value, the initially formed oxide film is broken down, and then plasma discharge occurs, resulting in the formation of PEO coating [14,15]. During this process, various processes are involved, including chemical, electrochemical, thermochemical, and plasma chemistry reactions [16]. Generally, this in-situ formed ceramic-like coating is well adherent to the substrate and has good wear resistance and corrosion resistance [17]. However, the tribological performance of the PEO coating fabricated on titanium alloy still needs to be further improved during the service under severe conditions. Additionally, the corrosion performance of the PEO coating also needs to be clarified when the alloy serves in a marine environment.

So far, parameters that affect the properties of the PEO coating have been studied, such as metal

Corresponding author: Lian-kui WU, E-mail: wulk5@mail.sysu.edu.cn; Fa-he CAO, E-mail: caofh5@mail.sysu.edu.cn
DOI: 10.1016/S1003-6326(22)66096-5

matrix [18], power parameters [19,20], electrolyte composition [21−24], additives [25], and electrolyte temperature [26]. Among them, the electrolyte composition has a great influence on the morphology and properties of the PEO coating. Silicate-, phosphate-, and aluminate-based electrolytes are the most commonly used electrolyte systems in the field of PEO. SHOKOUHFAR et al [21] reported that compared to the PEO coating fabricated from silicate-based electrolyte, the coating prepared from phosphate-based electrolyte had higher spark voltage, larger surface pores, and better corrosion resistance. WANG et al [22] found that with the increase of $NaAlO_2$ concentration in the electrolyte, the corrosion rate of the PEO coating prepared on pure titanium decreased first and then increased. MALINOVSCHI et al [23] investigated the influence of $NaAlO_2$ concentration on the microstructure, mechanical properties, and electrochemical behavior of PEO coatings formed on pure titanium. Results showed that the increase of $NaAlO_2$ concentration in the electrolyte is beneficial to increasing the hardness and thickness of the PEO coating. However, to the best of our knowledge, most of the researches were focused on improving the corrosion resistance of titanium alloys, and less attention is paid to the influence of electrolyte composition on the wear resistance of the PEO coating.

In the present work, four commonly-used electrolytes ($NaAlO_2$, Na_3PO_4, NaH_2PO_2, and Na_2SiO_3) were employed to systematically investigate the influence of electrolyte composition on the microstructure, composition, corrosion performance, and tribological behavior of PEO coating prepared on TC4 alloy. To fabricate a PEO coating with satisfying corrosion resistance and wear resistance, plasma electrolytic oxidation was performed in the electrolyte containing $NaAlO_2$ and NaH_2PO_2. This work not only provides support for further optimization of the PEO electrolyte to obtain high-quality PEO coating on titanium alloy but also provides an ideal for the preparation of PEO coating on other alloys.

2 Experimental

2.1 Materials

The TC4 specimen (20 mm × 20 mm × 5 mm) was polished with 220# silicon carbide sandpaper, ultrasonically cleaned in degreaser and deionized water for 5 min, respectively, and then dried with air. All chemicals were used without further purification and the electrolytes were prepared with deionized water.

2.2 Preparation of PEO coating

A pulsed power supply (NHWYDM800−5, China) was employed to prepare PEO coatings with a frequency of 1000 Hz, a current density of 5 A/dm^2, and a duty cycle of 60%. The PEO lasted for 20 min. The electrolyte used for the preparation of PEO coating was composed of 2.0 g/L NaOH, 2.0 g/L phenol (C_6H_5OH), and 10.0 g/L sodium salt ($NaAlO_2$, Na_3PO_4, NaH_2PO_2, or $Na_2SiO_3·5H_2O$, respectively). The PEO coatings fabricated from the electrolyte containing $NaAlO_2$, Na_3PO_4, NaH_2PO_2, and $Na_2SiO_3·5H_2O$ were defined as PEO-Al coating, PEO-HP coating, PEO-LP coating, and PEO-Si coating, respectively. An electrolyte containing 2.0 g/L NaOH, 2.0 g/L C_6H_5OH, 10.0 g/L NaH_2PO_2, and 10.0 g/L $NaAlO_2$ was employed to fabricate a composited coating, which is defined as PEO-Al-LP coating. Table 1 lists the detailed electrolyte composition and PEO condition of each coating.

Table 1 Electrolyte and parameters used in preparation of PEO coating

Specimen	Electrolyte	Parameter
PEO-Al	2.0 g/L NaOH, 2.0 g/L C_6H_5OH, and 10.0 g/L $NaAlO_2$	Frequency: 1000 Hz Current density: 5 A/dm^2 Duty cycle: 60% Anodization time: 20 min
PEO-HP	2.0 g/L NaOH, 2.0 g/L C_6H_5OH, and 10.0 g/L Na_3PO_4	
PEO-LP	2.0 g/L NaOH, 2.0 g/L C_6H_5OH, and 10.0 g/L NaH_2PO_2	
PEO-Si	2.0 g/L NaOH, 2.0 g/L C_6H_5OH, and 10.0 g/L $Na_2SiO_3·5H_2O$	
PEO-Al-LP	2.0 g/L NaOH, 2.0 g/L C_6H_5OH, 10.0 g/L $NaAlO_2$, and 10.0 g/L NaH_2PO_2	

During the PEO process, the TC4 alloy was used as the anode, and two pieces of stainless-steel plates were used as the cathodes. A stirring and cooling system was employed to make sure that the electrolyte temperature was lower than 30 °C. After

PEO, the specimen was taken out from electrolyte, rinsed with deionized water to remove the residual electrolyte, and then naturally dried in air.

2.3 Experiment

The thickness of the PEO coating was measured by a coating thickness gauge based on the eddy current principle (TIME2501, China). The data were taken from three parallel specimens. Ten measurements were carried out on each specimen, and the final value data were derived from the average value.

The microhardness of the PEO coating was measured by a digital microscopic Vickers hardness tester (HVS−1000). The load was 9.8 N and the holding time was 10 s. The data were taken from three parallel specimens. Three measurements were carried out on each specimen, and the final value data were derived from the average value.

Top-surface and cross-sectional morphologies of the PEO coating were characterized by a field emission scanning electron microscope (SEM, Quanta 400F, FEI, USA) equipped with energy dispersive spectroscopy (EDS). X-ray diffractometer (XRD, Empyrean, PANalytical) was used to determine the phase composition of PEO coatings using a Cu K_α radiation (λ=0.154056 nm) at 40 kV and 40 mA. The X-ray photoelectron spectroscopy (XPS, ESCALAB 250, Thermo-VG Scientific, USA) was employed to analyze the surface composition of the PEO coatings.

The corrosion behavior of the PEO coating was evaluated on an electrochemical workstation (CHI760E, CH Instruments, China) in 3.5 wt.% NaCl solution. A three-electrode system was used in the experiment. Saturated calomel electrode (SCE) was used as the reference electrode, a platinum plate was used as the counter electrode, and the PEO coating specimen or TC4 sample without coating was used as the working electrode. All specimens were immersed in 3.5 wt.% NaCl solution for 30 min before the polarization tests. The polarization measurement was carried out in the range from −500 mV (vs OCP) to +1500 mV (vs SCE) with a scan rate of 1.0 mV/s.

The tribological performance of the PEO coating was characterized by the high-speed reciprocating friction and wear tester (MDW−02G, Jinan Yihua, China) with a GCr15 steel ball of 6.35 mm in diameter as the counterpart. With a frequency of 1 Hz and an oscillating amplitude of 10 mm, a load of 5 N was applied for 20 min. After the test, the specimen was ultrasonic cleaned in deionized water for 5 min and dried naturally in the air. And the morphology and profile of the wear tracks were characterized by SEM and confocal microscopy (DVM6M, Leica, Germany).

3 Results and discussion

3.1 Evolution of cell voltage of PEO coatings

The evolution of the cell voltages during the preparation of the PEO coatings from four electrolyte systems is recorded in Fig. 1. It is revealed that the growth of the PEO-Al, PEO-LP, and PEO-Si coatings can be divided into three stages. At the first stage (Stage I), the cell voltage increases almost linearly with a high slope, corresponding to the anodization process. When reaching the breakdown voltage, the PEO enters the second stage (Stage II). At this stage, the increase of the voltage begins to slow down and small white sparks emerge on the alloy surface. With the prolonging of oxidation, the color of the sparks gradually turns to be yellow, and the number of the sparks increases. At the third stage (Stage III), the voltages keep at relatively stable values and the arc spots uniformly distribute on the alloy surface, accompanied by a strong popping sound [27]. For the PEO-HP coating, however, another stage can be found (Stage IV). In detail, the voltage declines sharply and the arc starts to gradually extinguish after oxidation for ~900 s. After that, large-area spark discharge disappears and the sparking is

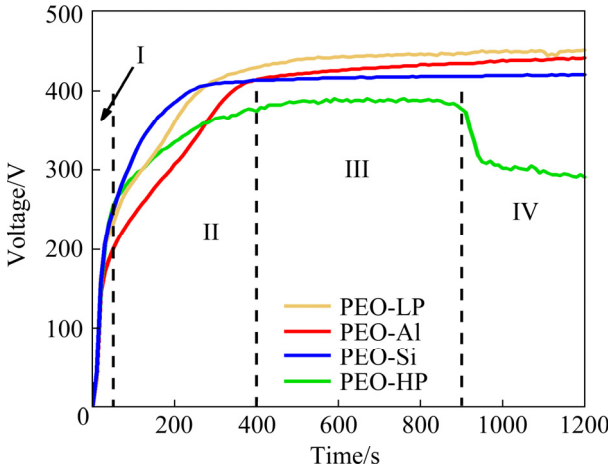

Fig. 1 Evolution of cell voltage during preparation of different PEO coatings

intermittent at local regions [28]. It has been reported that among the above four stages, the third stage is of great importance for the growth of the PEO coating and has a significant influence on the thickness, quality, and performance of the coating [2,29].

The energy (voltage) is a key factor affecting the growth of PEO coating [30]. The voltages at Stage III for the four electrolyte systems are ranked as follows: PEO-LP (~450 V) > PEO-Al (435−440 V) > PEO-Si (~420 V) > PEO-HP (390−400 V). Generally, the higher voltage represents the higher pulse energy and the greater discharge intensity, therefore benefiting the formation of a much thicker coating [31]. However, as shown in Fig. 2, the thickness of the PEO coatings is ranked as follows: PEO-LP > PEO-HP > PEO-Al ≈ PEO-Si, which is not consistent with the cell voltage sequence at Stage III. This phenomenon is attributed to two aspects. On the one hand, the actual voltage applied to the electrolyte is various for different electrolytes due to different conductivities [32]. Therefore, the actual voltage applied to the specimen deviates from the apparent cell voltage. On the other hand, the composition and surface structure of the PEO coatings fabricated in different electrolytes are different from each other, which will also affect the cell voltage. GUAN et al [32] demonstrated that the thickness and compactness of the coating had no obvious relevance with the V–t curve, while the composition and surface structure of the coating were highly related to the V–t curve. Other researchers also observed this phenomenon. VENKATESWARLU et al [33] fabricated titania (F-TiO_2) films on commercially pure titanium from four fluorine-containing electrolytes. The results showed that the stable voltage during PEO was ranked as follows: KTF ($Na_3PO_4·12H_2O$, K_2TiF_6, and KOH) > NF ($Na_3PO_4·12H_2O$, NH_4F, and KOH) > KF ($Na_3PO_4·12H_2O$, KF, and KOH) > NaF ($Na_3PO_4·12H_2O$, NaF, and KOH), while the order of thickness was ranked as follows: NaF > KF > NF > KTF.

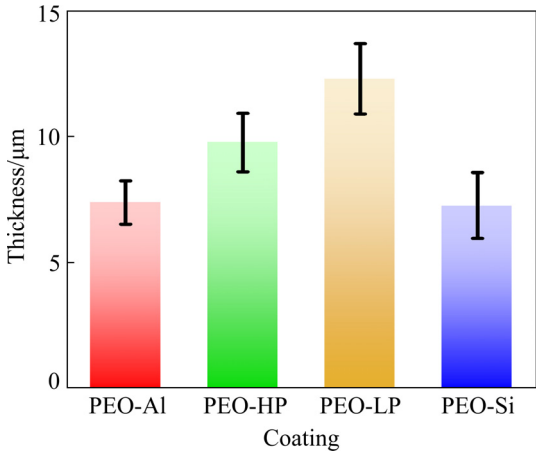

Fig. 2 Thickness of PEO coatings prepared from different electrolytes

3.2 Microstructure and composition of PEO coatings

3.2.1 Microstructure of PEO coatings

Figure 3 illustrates the top-surface SEM images of the PEO coatings prepared from four electrolytes. It can be noted that plenty of crater-like micropores are found on all PEO coatings, which are formed due to the molten oxide and gas bubbles throwing out from the micro-arc discharge channels [15]. Besides, the walls of the micropores are full of small pores. Moreover, the inhomogeneous stress distribution during the formation of the coating results in the generation of some cracks on the PEO coatings [5,34]. Interestingly, there are many granular protrusions in the PEO-Si coating. These protrusions are derived from the discharge process and molten material ejected from the discharge channels [35].

The chemical composition of the PEO coatings was analyzed by EDS. As given in Table 2, the oxygen content of all PEO coatings exceeds 65%, indicating that all PEO coatings are dominated by oxides [15]. Besides, the coating composition is highly dependent on the electrolyte composition. Specifically, the Al content in the PEO-Al coating is 25.14%, while it is less than 2% in the other three coatings. The P contents are 4.65% and 7.62% in the PEO-HP and PEO-LP coatings, respectively. And 15.41% Si is detected from the PEO-Si coating. These demonstrate that the formation of PEO coating is the result of the oxidation of the TC4 substrate and deposition of electrolyte-borne compounds [15].

Figure 4 shows the cross-sectional SEM images and the corresponding EDS composition of the four PEO coatings. It is revealed that the PEO-Al, PEO-HP, and PEO-LP coatings have a two-layer structure, while the PEO-Si coating has no obvious delamination characteristic. The outer layer exhibits a porous structure while the inner layer is relatively dense. Generally, the inner layer

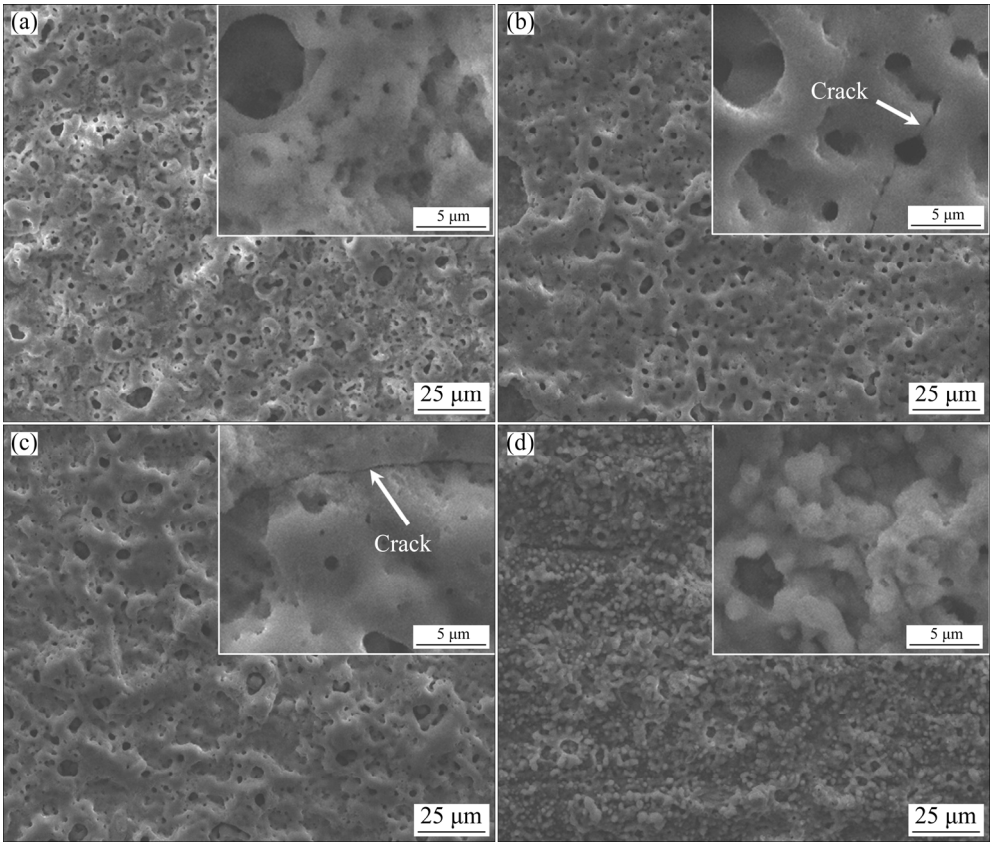

Fig. 3 Top-surface SEM images of PEO coatings: (a) PEO-Al; (b) PEO-HP; (c) PEO-LP; (d) PEO-Si

Table 2 Chemical compositions of top surface of PEO coatings

Coating	Element content/at.%					
	Ti	Al	V	O	P	Si
PEO-Al	7.74	25.14	−	67.12	−	−
PEO-HP	22.56	1.96	0.44	70.39	4.65	−
PEO-LP	18.58	1.55	0.66	71.59	7.62	−
PEO-Si	11.33	1.52	0.24	71.50	−	15.41

plays an important role in preventing inward diffusion of corrosion medium to the substrate. Unfortunately, some micropores are found in the inner layer of the PEO-Al and PEO-HP coatings. And the PEO-Si coating with some micropores is very thin in some regions. Therefore, it can be deduced that the PEO-LP coating with a continuous and dense inner layer may provide good resistance against corrosion.

The elements mapping and linear distribution at the coating/substrate interface were also analyzed (Fig. 4). For the PEO-Al coating, the Al content of the coating near the substrate is much lower than that of the outer layer of the coating. The distributions of P and Si exhibit a similar phenomenon for the other three coatings. According to Ref. [36], the inner layer of the PEO coating is formed due to the electrochemical reactions caused by the applied voltage, and the outer layer with porous structure is generated due to the plasma interaction between the substrate and electrolyte. Hence, it can be concluded from the results that the growth of PEO coating mainly depends on the reactive deposition of the electrolyte composition.

3.2.2 Phase composition of PEO coatings

Figure 5 presents the XRD patterns of the four PEO coatings. The typical diffraction peak of α-Ti derived from the substrate is detected owing to the thin and porous structure of the coatings. Meanwhile, both rutile and anatase TiO_2 are identified from all PEO coatings. However, no diffraction peak related to elements of P and Si is observed. Combined with the XRD results and EDS analysis (Table 2), it can be inferred that P and Si mainly exist in the form of an amorphous phase. A similar phenomenon has been also observed by other researchers [12,37]. In addition, it can be seen

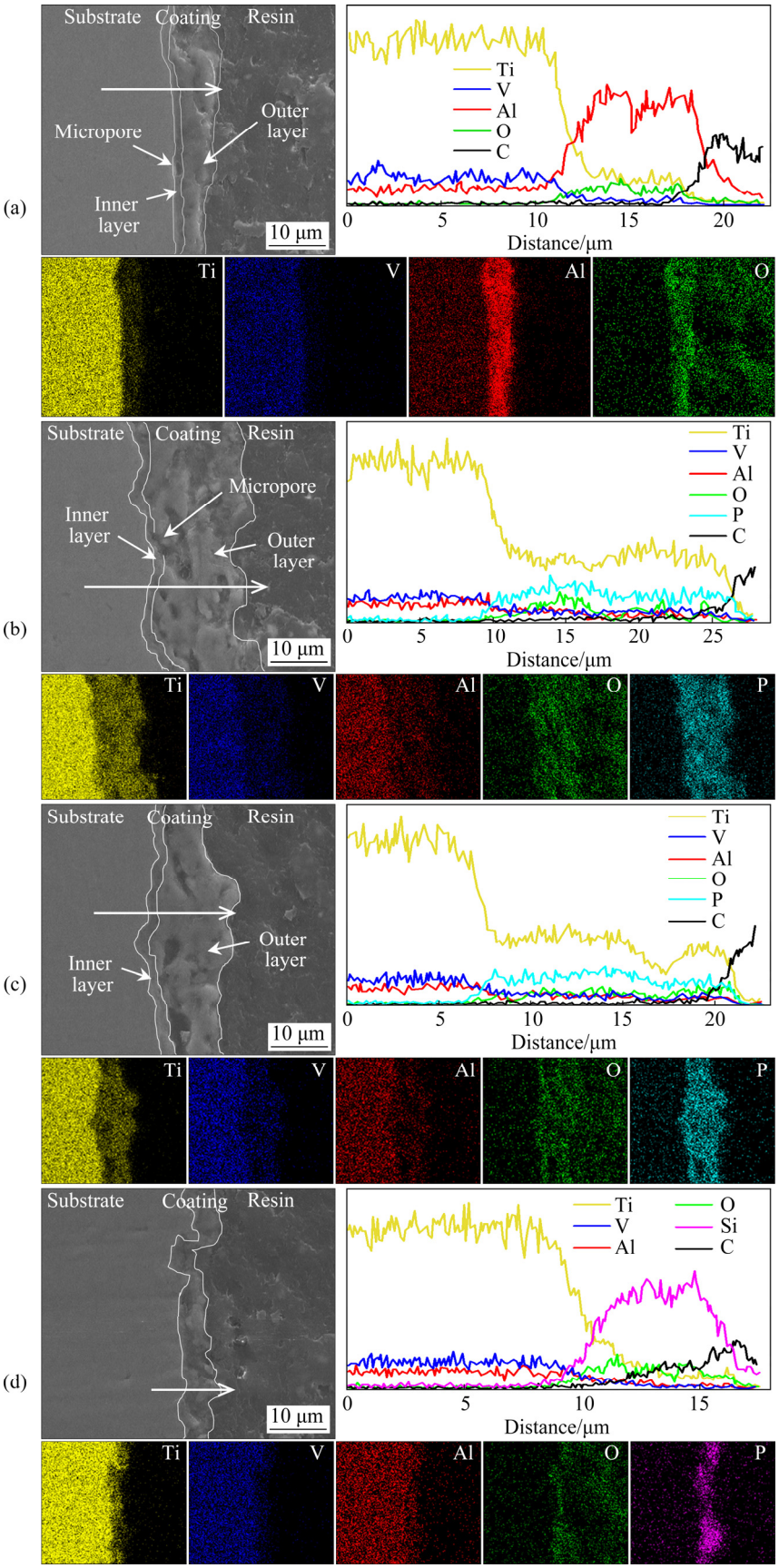

Fig. 4 Cross-sectional SEM images together with elements mapping and linear distribution of PEO coatings: (a) PEO-Al; (b) PEO-HP; (c) PEO-LP; (d) PEO-Si (The arrows marked in the images represent the direction and position of the elements line scan measurements carried out)

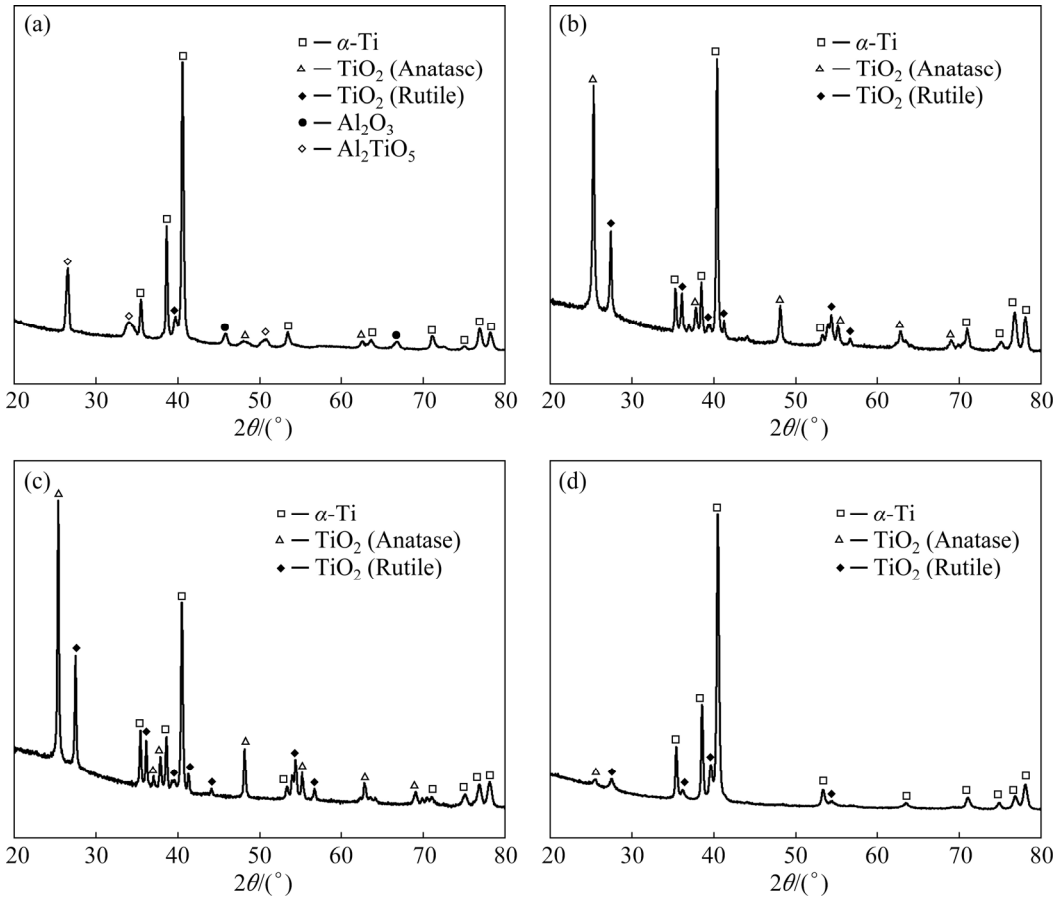

Fig. 5 XRD patterns of PEO coatings: (a) PEO-Al; (b) PEO-HP; (c) PEO-LP; (d) PEO-Si

that the diffraction intensities of rutile and anatase in PEO-Si coating are much weaker than those in the PEO-HP and PEO-LP coatings. This may be because the PEO-Si coating is very thin and the PEO-Si coating is mainly composed of silicate oxide.

For the PEO-Al coating, Al_2TiO_5 and Al_2O_3 are the dominant phases. The presence of Al_2TiO_5 indicates that the following reaction occurs during the PEO process [23,38]:

$$TiO_2+Al_2O_3 \rightarrow Al_2TiO_5 \quad (1)$$

YEROKHIN et al [39] also observed Al_2TiO_5 in the PEO coatings prepared from Al−Si ($KAlO_2$ and Na_2SiO_3) and Al−P ($KAlO_2$ and Na_3PO_4) electrolytes.

3.2.3 XPS spectra analysis of PEO coatings

XPS characterization was carried out to further determine the composition of the four coatings. As shown in the survey XPS spectra (Fig. 6(a)), Ti, Al, and O are detected from all coatings. Additionally, P is detected from the PEO-HP and PEO-LP coatings, while Si is found in the PEO-Si coating.

As for the high-resolution Ti 2p spectra (Fig. 6(b)), two spin-orbit doubles located at 459.05 and 464.75 eV are characteristics of Ti $2p_{3/2}$ and Ti $2p_{1/2}$ [12]. The difference in the binding energy between the two peaks is 5.70 eV, which is consistent with the previously-reported spin-orbit splitting value for TiO_2 [12]. However, for the PEO-Al coating (Fig. 6(b)), two other spin-orbit doubles located at 463.71 and 458.22 eV are observed, indicating the presence of Al_2TiO_5 [40]. Figure 6(c) shows the high-resolution Al 2p spectra of the PEO coatings. For the PEO-Al coating, the Al 2p spectra can be deconvoluted into two peaks at 74.85 and 73.90 eV, which can be assigned to Al_2O_3 and Al_2TiO_5, respectively [41]. With a low signal-to-noise ratio, the Al 2p spectra of the other three PEO coatings can be fitted with one peak, corresponding to Al_2O_3 [32]. As displayed in Fig. 6(d), the binding energies of P 2p spectra in the PEO-HP and PEO-LP coatings are centered at 133.73 and 133.80 eV, respectively, which can be assigned to PO_4^{3-} [12]. The Si 2p spectra of the PEO-Si coating present only one peak at the

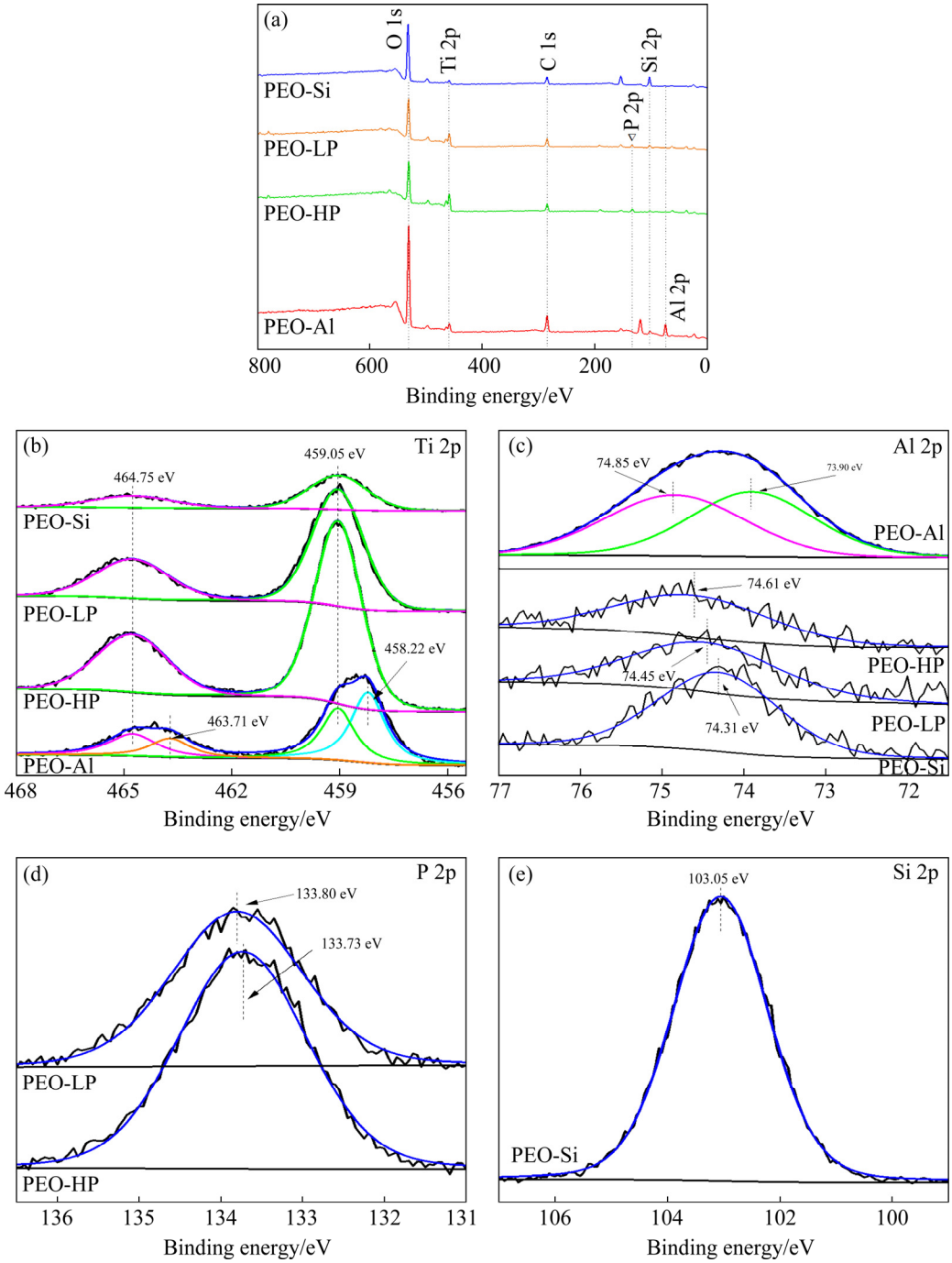

Fig. 6 Survey XPS spectra (a) and high resolution XPS spectra of Ti 2p (b), Al 2p (c), P 2p (d), and Si 2p (e) of PEO coatings

binding energy of 103.05 eV (Fig. 6(e)), indicating the presence of SiO_2 [42].

3.3 Corrosion behavior of PEO coatings

As shown in Fig. 7, the polarization curve collected from 3.5 wt.% NaCl solution at room temperature was employed to evaluate the corrosion performance of the PEO coatings. The corrosion potential (φ_{corr}) and corrosion current density (J_{corr}) derived from the Polarization curves are listed in Table 3. Results show that the corrosion potential of all PEO coatings is more positive than that of the bare TC4 alloy, indicating that PEO is beneficial to improving the thermodynamic stability of TC4 alloy [36]. Meanwhile, the corrosion current density of TC4 alloy is dramatically reduced by one order or two orders of magnitude after the PEO treatment, manifesting the improved corrosion resistance. This

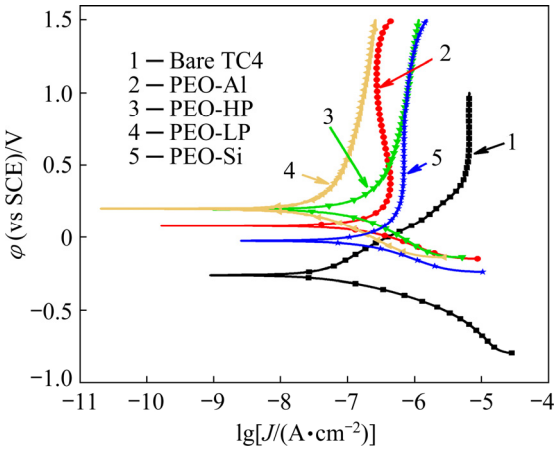

Fig. 7 Polarization curves of bare TC4 alloy and PEO coatings

Table 3 Parameters derived from polarization curves in Fig. 7

Coating	φ_{corr} (vs SCE)/V	J_{corr}/(A·cm^{-2})
Bare TC4	−0.263	1.25×10^{-6}
PEO-Al	0.08	1.53×10^{-7}
PEO-HP	0.194	1.06×10^{-7}
PEO-LP	0.2	2.88×10^{-8}
PEO-Si	−0.025	1.66×10^{-7}

is because the thickness of the PEO coating is obviously larger than that of the nature passivation film, whose thickness is 1.5−10 nm [18]. Moreover, the current density of the PEO coatings at the anodic branches is much lower than that of the bare TC4 alloy, suggesting that the PEO coating could efficiently impede the anodic reaction and protect the substrate from corrosion attack. The order of corrosion current density of the four PEO coatings is as follows: PEO-LP < PEO-HP < PEO-Al < PEO-Si. The PEO-LP coating exhibits the lowest corrosion current density, indicating the best corrosion resistance. And this result is consistent with the cross-sectional SEM image (Fig. 4). The inferior corrosion resistance of the PEO-Al and PEO-Si coatings may be attributed to the non-compact coating/substrate interface structure and small coating thickness.

3.4 Tribological performance of PEO coatings

Figure 8 shows the evolution of the friction coefficients of TC4 alloy and PEO coatings tested under dry sliding conditions. It can be seen that the friction coefficient of the PEO-Al and PEO-HP coatings is similar to that of the TC4 alloy, and all of them fluctuate at ~0.2, whereas the friction coefficient of the PEO-LP coating is slightly higher and fluctuates at ~0.3. The large fluctuations of the friction coefficients can be attributed to the volcanic micropores on the surface of the PEO coatings (Fig. 3) [36]. Notably, the PEO-HP and PEO-LP coatings are destroyed in a few seconds. Meanwhile, it is notable that the friction coefficient of the PEO-Si coating drops sharply when the wear test is conducted for 700 s, suggesting that the PEO-Si coating is completely destroyed by the counterpart at this moment. This suggests that the wear resistance of the PEO-HP and PEO-LP coatings is inferior to that of the PEO-Al and PEO-Si coatings.

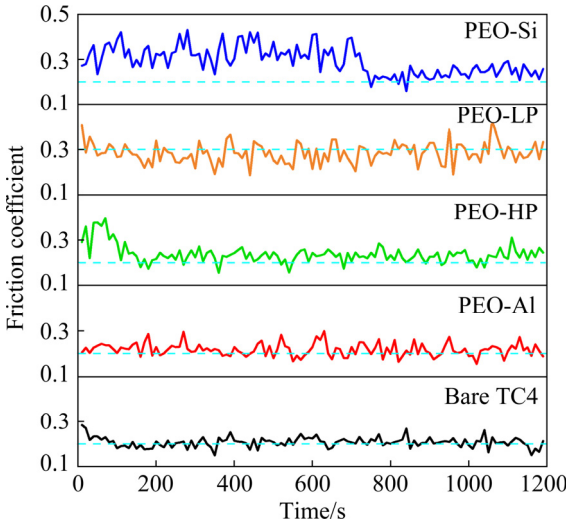

Fig. 8 Evolution of friction coefficients of bare TC4 alloy and PEO coatings

After the wear test, the surface morphology, 3D topography, and chemical composition of the coatings were characterized by SEM, confocal microscopy, and EDS, respectively. As shown in Fig. 9, obvious wear tracks are observed on bare TC4 alloy and all PEO coatings. Additionally, the PEO-HP, PEO-LP, and PEO-Si coatings are completely destroyed and the substrate beneath the coating is also severely worn. Despite this, the width of the wear track in the PEO-Si coating is narrower than that of the PEO-HP and PEO-LP coatings. Meanwhile, plenty of abrasive grooves and some adhesive peeled pits can be observed. Despite this, the adhesive peeled pits on PEO-HP, PEO-LP, and PEO-Si coatings are much less than those on TC4 alloy. It can be concluded that the dominant wear mechanism of bare TC4 alloy,

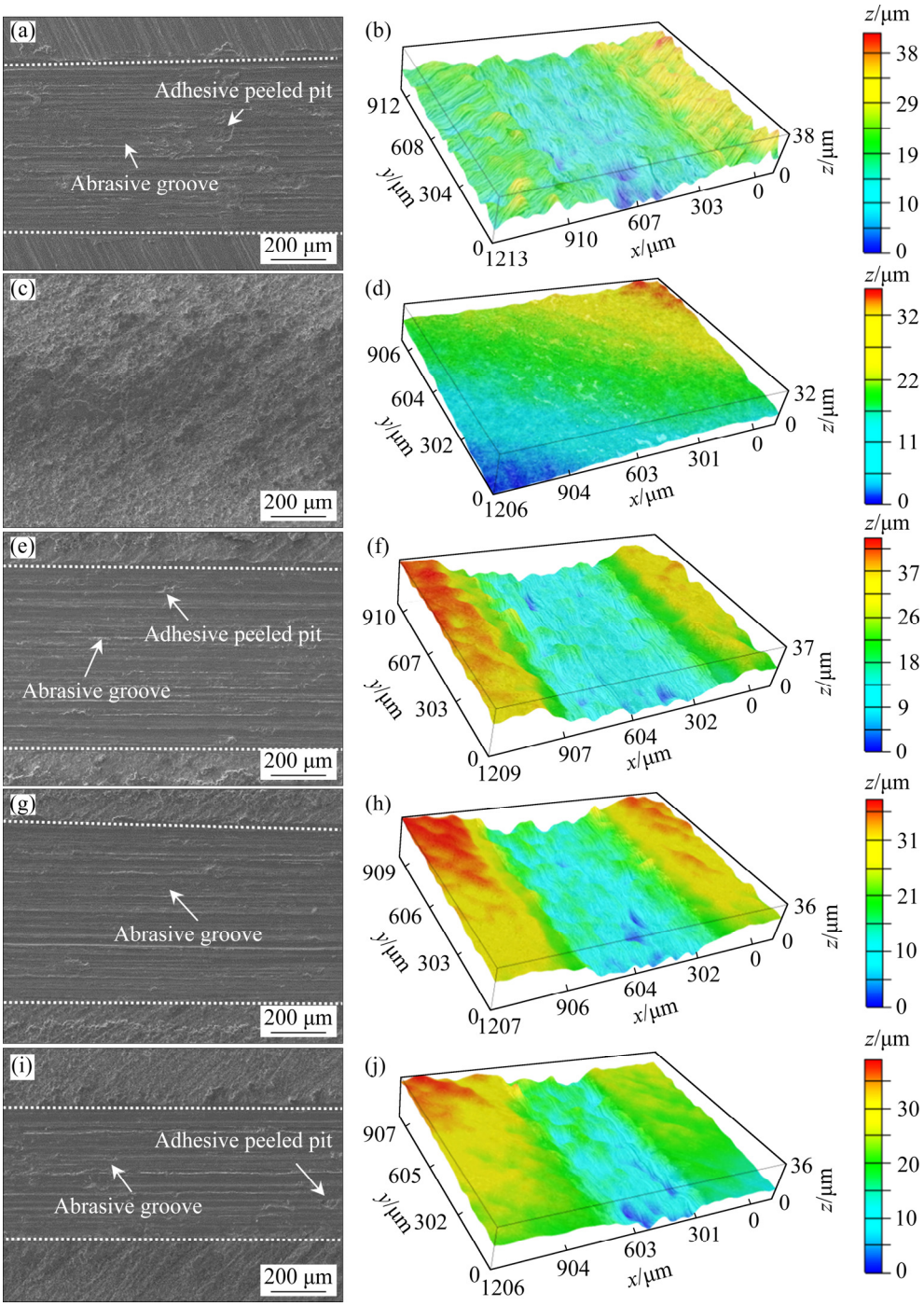

Fig. 9 SEM images and 3D topographies of bare TC4 alloy (a, b) and PEO coatings (c–j) after wear test: (c, d) PEO-Al; (e, f) PEO-HP; (g, h) PEO-LP; (i, j) PEO-Si

PEO-HP, PEO-LP, and PEO-Si coatings is abrasive wear, accompanied by the adhesive wear [43]. Interestingly, only a few wear marks are observed on the surface of PEO-Al coating and no obvious abrasive grooves and adhesive peeled pits are found, indicating that only slight wear damage occurs during the sliding test.

The chemical compositions of the wear tracks in the PEO coatings are displayed in Table 4. Si, C, and Fe derived from the GCr15 steel counterpart are detected from the wear track of the PEO-Al coating, indicating the formation of the transfer layer during the friction process [11]. However, only Ti, Al, and V are detected from the wear tracks of the PEO-HP and PEO-LP coatings. This manifests that the PEO-HP and PEO-LP coatings

are destroyed by the GCr15 steel counterpart, resulting in the exposure of the TC4 substrate. As for the PEO-Si coating, besides Ti, Al, and V, tiny Si is also detected.

Table 4 Chemical compositions of wear scar area

Coating	Element content/at.%						
	Ti	Al	V	O	Si	C	Fe
PEO-Al	4.87	17.29	0.26	63.57	0.29	6.17	7.55
PEO-HP	85.39	11.09	3.51	−	−	−	−
PEO-LP	86.37	10.30	3.32	−	−	−	−
PEO-Si	85.33	10.76	3.43	−	0.49	−	−

To further investigate the tribological behavior of the PEO coatings, the depth profile of the wear tracks and the wear rate of the PEO coatings were characterized (Fig. 10). It is obvious that the wear track depths are various from each other (Fig. 10(a)). The order of the wear tracks depth of the four coatings is as follows: PEO-Al < PEO-Si < PEO-HP ≈ PEO-LP. And it can be noted that the depth of PEO-HP, PEO-LP, and PEO-Si coatings is much greater than their thickness, indicating that these coatings have poor wear resistance. This is consistent with the SEM images (Fig. 9).

The wear rate is (ω) calculated by dividing the volume of the wear track (V/mm^3) by testing load (F/N) and total sliding distance (L/m) [25]:

$$\omega=V/(F\cdot L) \quad (2)$$

As shown in Fig. 10(b), the wear resistance of four coatings is ranked as follows: PEO-Al > PEO-Si > PEO-LP > PEO-HP. In detail, the wear rates of PEO-Al, PEO-HP, PEO-LP, and PEO-Si coatings are 7.5×10^{-5}, 1.2×10^{-3}, 9.9×10^{-4}, and 6.6×10^{-4} mm$^3\cdot$N$^{-1}\cdot$m^{-1}, respectively. The wear rate of PEO-Al coating is only 10.4% that of the bare TC4 alloy, which has the best wear resistance among the four coatings. The hardness of the PEO coating was also measured. As shown in Fig. 11, PEO treatment is beneficial to improving the hardness of the alloy. In detail, the hardness values of bare TC4, PEO-Al, PEO-HP, PEO-LP, and PEO-Si coatings are HV 303, HV 480, HV 353, HV 401, and HV 440, respectively. The PEO-Al coating reveals the highest hardness because the PEO-Al coating contains Al_2O_3 (Vickers microhardness: HV 2085 [25]) and Al_2TiO_5 [24]. Moreover, Al_2O_3 also has high fracture strength

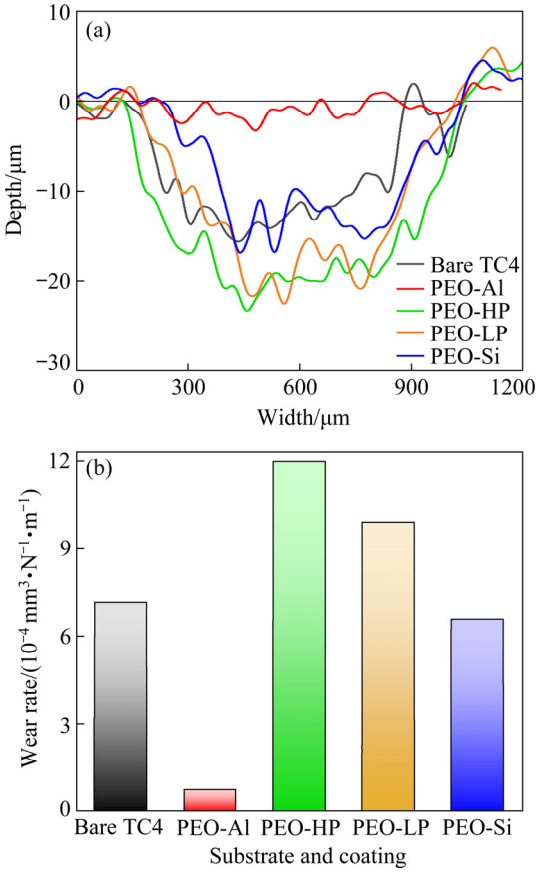

Fig. 10 Profiles (a) and wear rates (b) of bare TC4 alloy and PEO coatings after wear test

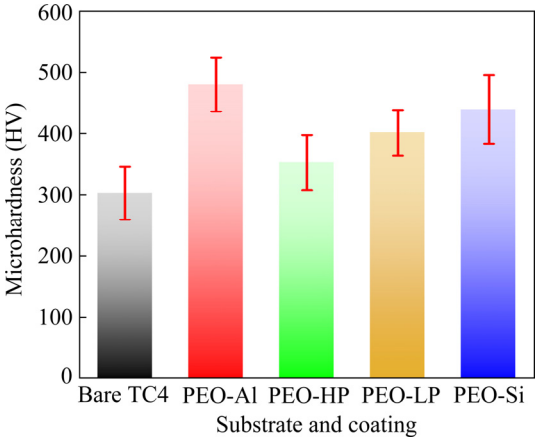

Fig. 11 Microhardness of bare TC4 alloy and PEO coatings prepared from different electrolytes

(282−1084 MPa) and high fracture toughness (3.5−5.2 MPa·m$^{1/2}$) [25], which can improve the wear resistance of the coating. Due to the loose structure, the hardness of the PEO-HP coating is lower than that of PEO-LP [44].

The schematic diagram of friction between PEO-Al coating and GCr15 counterpart ball is shown in Fig. 12(a). Because the hardness of the

coating is higher than that of the counterpart ball, no obvious damage emerges during the grinding. The schematic diagram of friction between the other three coatings and the GCr15 counterpart ball is illustrated in Fig. 12(b). With the porous structure and relatively low hardness, these PEO coatings wear out quickly when ground by a relatively harder counterpart ball. For the PEO-Si coating, because the outmost layer is full of particles and the depth of the micropores is relatively shallow, the worn debris can be filled into the micropores to increase the contact area and reduce the unit area lords [36,45], therefore exhibiting better wear resistance than PEO-HP and PEO-LP coatings.

Based on the above results, it can be concluded that among the four PEO coatings, the PEO-LP coating exhibits the best corrosion resistance, while the PEO-Al coating performs the highest wear resistance. To prepare PEO coating with good corrosion resistance and wear resistance, a composite coating, defined as PEO-Al-LP coating was fabricated from an electrolyte containing NaH_2PO_2 and $NaAlO_2$.

Figure 13(a) displays the SEM image of the PEO-Al-LP coating. Obviously, the coating still shows a crater-like morphology. The pore size distribution of PEO coatings is shown in Fig. 14. The region for calculating the pore size distribution of the PEO coating is randomly selected and analyzed by ImageJ [46]. It can be found that the pore size of all three coatings is mostly distributed within 1 μm, but it is not negligible for the PEO-Al and PEO-LP coatings which have larger pores (>6 μm), while the size of the pore in the PEO-Al-LP coating is less than 4 μm. EDS analysis indicates that 11.61% Ti, 17.37% Al, 0.22% V, 69.25% O, and 1.55% P are detected from the coating (Fig. 13(b)). XRD analysis indicates that besides the α-Ti derived from the substrate, anatase, rutile, Al_2TiO_5, and Al_2O_3 can be identified from the PEO-Al-LP coating (Fig. 13(c)). Based on the EDS analysis and XRD result, it can be confirmed that the Al and P-based composite coating has been successfully prepared.

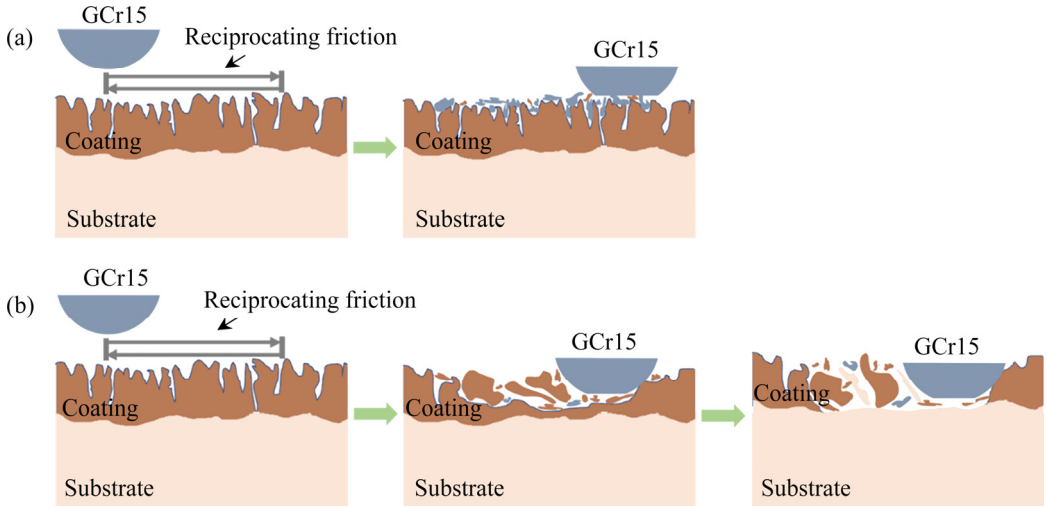

Fig. 12 Schematic diagrams of friction between GCr15 counterpart ball and PEO coating: (a) PEO-Al coating; (b) PEO-HP, PEO-LP, and PEO-Si coatings

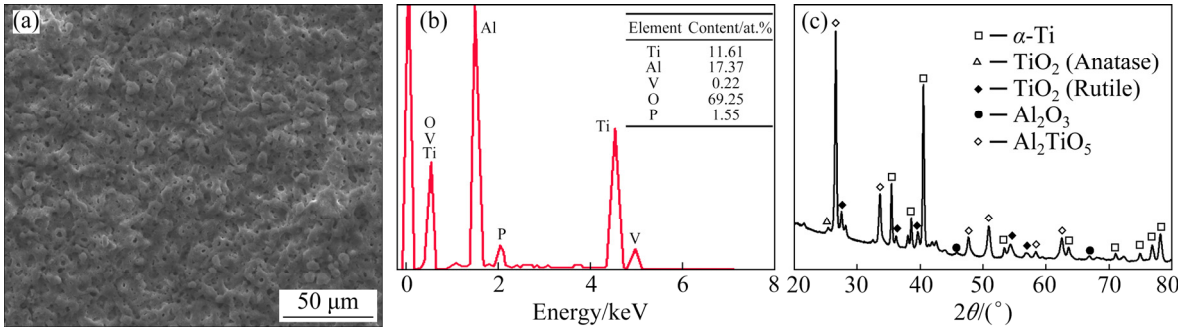

Fig. 13 SEM image (a), EDS results (b) and XRD pattern (c) of PEO-Al-LP coating

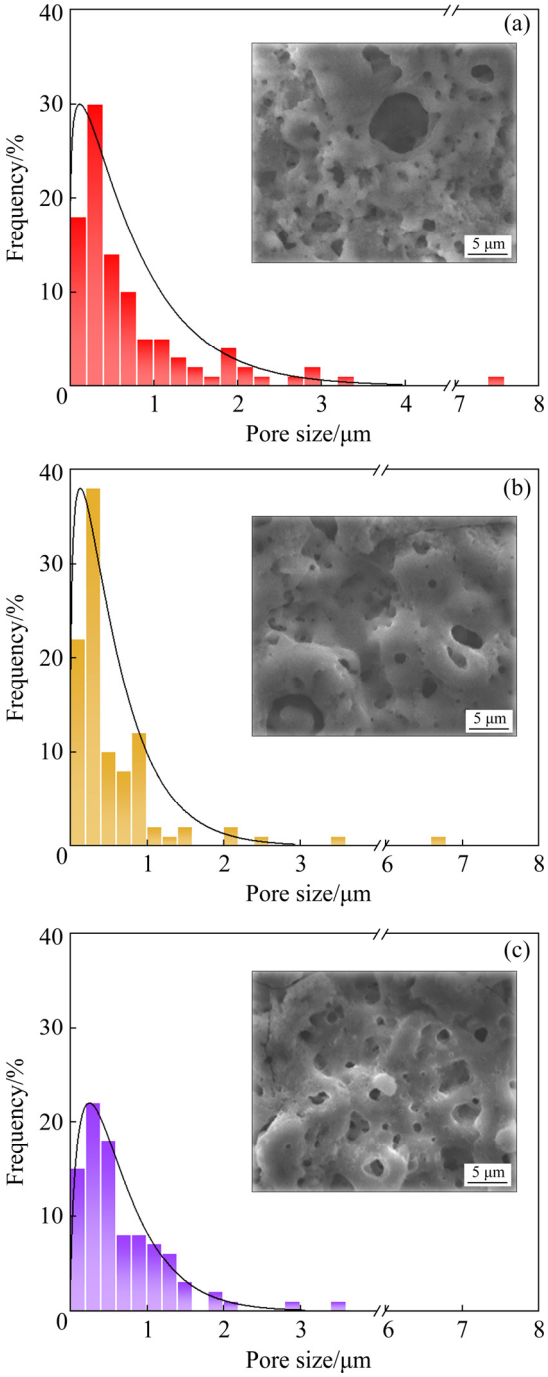

Fig. 14 Pore size distribution of PEO-Al coating (a), PEO-LP coating (b), and PEO-Al-LP coating (c) (The size distribution curve is obtained by fitting the gamma distribution)

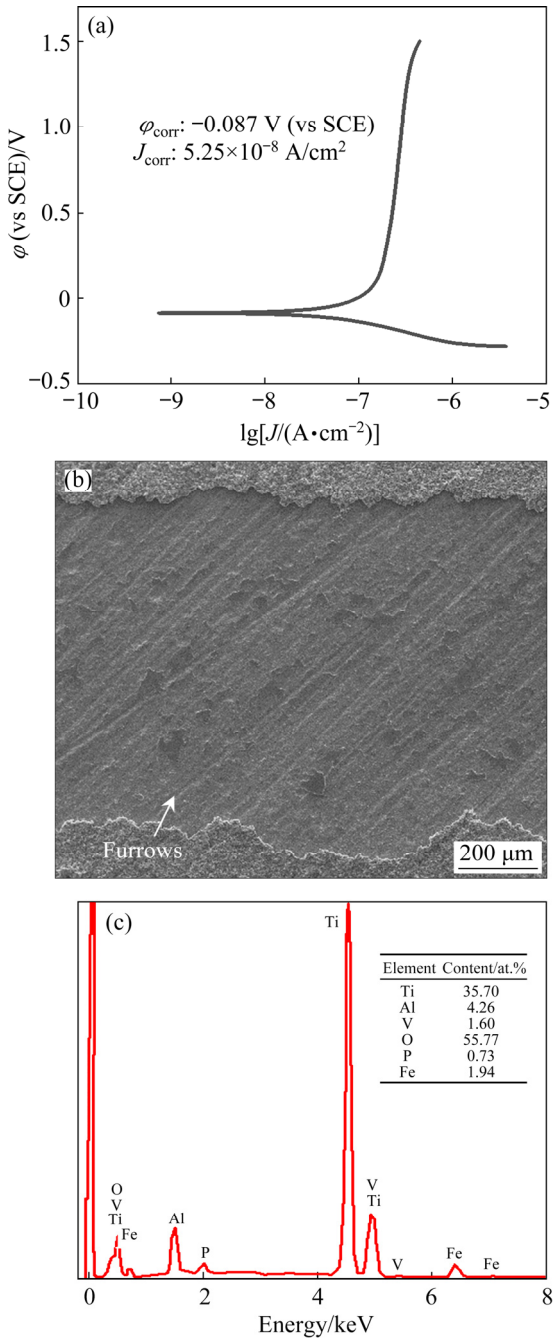

Fig. 15 Polarization curve of PEO-Al-LP coating (a), SEM image (b) and EDS results (c) of PEO-Al-LP coating after wear test

The corrosion behavior and tribological performance of the PEO-Al-LP coating were characterized. As shown in the polarization curve (Fig. 15(a)), the corrosion current density of the PEO-Al-LP coating is 5.25×10^{-8} A/cm^2, which is lower than that of the PEO-Al coating, indicating the improved corrosion resistance. SEM image indicates that after the wear test the crater-like micropores in the PEO-Al-LP coating disappear, and many obvious furrows emerge on the wear track (Fig. 15(b)). Interestingly, the direction of the furrows is not consistent with the direction of the sliding. Moreover, EDS analysis reveals that the wear track is oxygen-enriched and Fe is also detected (Fig. 15(c)). This indicates that the

PEO-Al-LP coating is not completely destroyed and a transfer layer is formed between the counterpart ball and the coating during the friction process. The wear resistance of the PEO-Al-LP coating is inferior to that of the PEO-Al coating but superior to that of the PEO-LP coating. Therefore, it can be concluded that optimization of the electrolyte composition can improve the overall performance of the PEO coating.

4 Conclusions

(1) PEO-Al, PEO-HP, and PEO-LP coatings show two-layered structures. The outer layer is porous, while the inner layer is dense. However, the PEO-Si coating has no obvious delamination structure and the surface of the PEO-Si coating is full of granular protrusions.

(2) The corrosion resistance of the TC4 alloy is improved by PEO. The PEO-LP coating exhibits the best corrosion resistance with the corrosion current density of 2.88×10^{-8} A/cm^2, which is two orders of magnitude lower than that of the bare TC4 alloy.

(3) The PEO-Al coating exhibits high microhardness and good wear resistance. No obvious abrasive grooves and adhesive peeled pits are found on the surface and the wear rate of the PEO-Al coating is as low as 7.5×10^{-5} mm$^3\cdot$N$^{-1}\cdot$m^{-1}, which is 10.4% that of bare TC4 alloy.

(4) The corrosion resistance of the PEO-Al-LP coating is superior to that of the PEO-Al coating, and the wear resistance of the PEO-Al-LP coating is superior to that of PEO-LP coating.

Acknowledgments

This work was financially supported by the National Natural Science Foundation of China (Nos. 52071347, 51971205), and the Innovation Group Project of Southern Marine Science and Engineering Guangdong Laboratory (Zhuhai), China (No. 311020012).

References

[1] GEETHA M, SINGH A K, ASOKAMANI R, GOGIA A K. Ti based biomaterials, the ultimate choice for orthopaedic implants—A review [J]. Progress in Materials Science, 2009, 54: 397−425.

[2] TU Zhen-mi, LI Ning, ZHU Yong-ming. Application and technology on surface treatment of titanium and titanium alloys [M]. China: National Defense Industry Press, 2010.

[3] ZHAI Da-jun, FENG Ke-qin. Preparation of micro/nano-structured ceramic coatings on Ti6Al4V alloy by plasma electrolytic oxidation process [J]. Transactions of Nonferrous Metals Society of China, 2019, 29: 2546−2555.

[4] YANG Xin, WANG Wan-lin, MA Wen-jun, WANG Yan, YANG Jun-gang, LIU Shi-feng, TANG Hui-ping. Corrosion and wear properties of micro-arc oxidation treated Ti6Al4V alloy prepared by selective electron beam melting [J]. Transactions of Nonferrous Metals Society of China, 2020, 30: 2132−2142.

[5] MASHTALYAR D V, NADARAIA K V, IMSHINETSKIY I M, BELOV E A, FILONINA V S, SUCHKOV S N, SINEBRYUKHOV S L, GNEDENKOV S V. Composite coatings formed on Ti by PEO and fluoropolymer treatment [J]. Applied Surface Science, 2021, 536: 147976.

[6] CESCHINI L, LANZONI E, MARTINI C, PRANDSTRALLER D, SAMBOGNA G. Comparison of dry sliding friction and wear of Ti6Al4V alloy treated by plasma electrolytic oxidation and PVD coating [J]. Wear, 2008, 264: 86−95.

[7] SHAMRAY V F, SIROTINKIN V P, SMIRNOV I V, KALITA V I, FEDOTOV A Y, BARINOV S M, KOMLEV V S. Structure of the hydroxyapatite plasma-sprayed coatings deposited on pre-heated titanium substrates [J]. Ceramics International, 2017, 43: 9105−9109.

[8] HSIAO W T, CHANG H C, NANCI A, DURAND R. Surface microtexturing of Ti−6Al−4V using an ultraviolet laser system [J]. Materials & Design, 2016, 90: 891−895.

[9] RAUTRAY T R, NARAYANAN R, KWON T Y, KIM K H. Surface modification of titanium and titanium alloys by ion implantation [J]. Journal of Biomedical Materials Research Part B: Applied Biomaterials, 2010, 93B: 581−591.

[10] WANG Y M, GUO L X, OUYANG J H, ZHOU Y, JIA D C. Interface adhesion properties of functional coatings on titanium alloy formed by microarc oxidation method [J]. Applied Surface Science, 2009, 255: 6875−6880.

[11] GUO Qiao-qin, XU Da-peng, YANG Wei, GUO Yong-chun, YANG Zhong, LI Jian-ping, GAO Pei-hu. Synthesis, corrosion, and wear resistance of a black microarc oxidation coating on pure titanium [J]. Surface and Coatings Technology, 2020, 386: 125454.

[12] MORTAZAVI G, JIANG J, MELETIS E I. Investigation of the plasma electrolytic oxidation mechanism of titanium [J]. Applied Surface Science, 2019, 488: 370−382.

[13] QIN Ying, WU Guo-hua, ATRENS A, ZHANG Xiao-long, ZHANG Liang, DING Wen-jiang. Effect of NaOH concentration on microstructure and corrosion resistance of MAO coating on cast Al−Li alloy [J]. Transactions of Nonferrous Metals Society of China, 2021, 31: 913−924.

[14] WALSH F C, LOW C T J, WOOD R J K, STEVENS K T, ARCHER J, POETON A R, RYDER A. Plasma electrolytic oxidation (PEO) for production of anodised coatings on lightweight metal (Al, Mg, Ti) alloys [J]. Transactions of the Institute of Metal Finishing, 2009, 87: 122−135.

[15] LI Qing-biao, YANG Wen-bin, LIU Can-can, WANG Dao-ai, LIANG Jun. Correlations between the growth mechanism and properties of micro-arc oxidation coatings on titanium

alloy: Effects of electrolytes [J]. Surface and Coatings Technology, 2017, 316: 162−170.

[16] CAI Jing-shun, CAO Fa-he, CHANG Lin-rong, ZHENG Jun-jun, ZHANG Jian-qing, CAO Chu-nan. The preparation and corrosion behaviors of MAO coating on AZ91D with rare earth conversion precursor film [J]. Applied Surface Science, 2011, 257: 3804−3811.

[17] MARTIN J, HARAUX P, NTOMPROUGKIDIS V, MIGOT S, BRUYÈRE S, HENRION G. Characterization of metal oxide micro/nanoparticles elaborated by plasma electrolytic oxidation of aluminium and zirconium alloys [J]. Surface & Coatings Technology, 2020, 397: 125987.

[18] FAZEL M, SALIMIJAZI H R, GOLOZAR M A, GARSIVAZ JAZI M R. A comparison of corrosion, tribocorrosion and electrochemical impedance properties of pure Ti and Ti6Al4V alloy treated by micro-arc oxidation process [J]. Applied Surface Science, 2015, 324: 751−756.

[19] WANG Ying-jun, WANG Lin, ZHENG Hua-de, DU Chang, NING Cheng-yun, SHI Zhi-feng, XU Cai-xia. Effect of frequency on the structure and cell response of Ca- and P-containing MAO films [J]. Applied Surface Science, 2010, 256: 2018−2024.

[20] TORRES-CERON D A, RESTREPO-PARRA E, ACOSTA-MEDINA C D, ESCOBAR-RINCON D, OSPINA-OSPINA R. Study of duty cycle influence on the band gap energy of TiO_2/P coatings obtained by PEO process [J]. Surface & Coatings Technology, 2019, 375: 221−228.

[21] SHOKOUHFAR M, DEHGHANIAN C, MONTAZERI M, BARADARAN A. Preparation of ceramic coating on Ti substrate by plasma electrolytic oxidation in different electrolytes and evaluation of its corrosion resistance: Part II [J]. Applied Surface Science, 2012, 258: 2416−2423.

[22] WANG Ping, WU Ting, PENG Hao, GUO Xiao-yang. Effect of $NaAlO_2$ concentrations on the properties of micro-arc oxidation coatings on pure titanium [J]. Materials Letters, 2016, 170: 171−174.

[23] MALINOVSCHI V, MARIN A, DUCU C, ANDREI V, COACA E, CRACIUM V, LUNGU M. Influence of sodium aluminate concentration and process duration on microstructure, mechanical and electrochemical behavior of PEO coatings formed on CP-Ti [J]. Surface & Coatings Technology, 2021, 418: 127240.

[24] WANG Hua-yue, LI Yun-yu, CHEN Zhao-xiang, CHAI Chen, GAO Shan. Optimization of preparation process and wear resistance of Ti micro-arc oxidation coatings [J]. Journal of Yanshan University, 2021, 45: 496−504. (in Chinese)

[25] MUHAFFEL F, KABA M, CENIPURA G, DERIN B, KRUK A, ATAR E, CIMENOGLU H. Influence of alumina and zirconia incorporations on the structure and wear resistance of titania-based MAO coatings [J]. Surface & Coatings Technology, 2019, 377: 124900.

[26] HABAZAKI H, TSUNEKAWA S, TSUJI E, NAKAYAMA T. Formation and characterization of wear-resistant PEO coatings formed on β-titanium alloy at different electrolyte temperatures [J]. Applied Surface Science, 2012, 259: 711−718.

[27] ZHANG Xin-xin, CAI G, LV You, WU Yu-le, DONG Ze-hua. Growth mechanism of titania on titanium substrate during the early stage of plasma electrolytic oxidation [J]. Surface & Coatings Technology, 2020, 400: 126202.

[28] WANG Yi, YU Hui-jun, CHEN Chuan-zhong, ZHAO Zhi-huan. Review of the biocompatibility of micro-arc oxidation coated titanium alloys [J]. Materials & Design, 2015, 85: 640−652.

[29] LIU Lin, YU Si-rong, ZHU Guang, LI Quan, LIU En-yang, XIONG Wei, WANG Bing-ying, YANG Xi-zhen. Corrosion and wear resistance of micro-arc oxidation coating on glass microsphere reinforced Mg alloy composite [J]. Journal of Materials Science, 2021, 56: 15379−15396.

[30] LI Xin-yi, DONG Chao-fang, ZHAO Qing, PANG Yu, CHENG Fa-song, WANG Shuai-xing. Characterization of microstructure and wear resistance of PEO coatings containing various microparticles on Ti6Al4V alloy [J]. Journal of Materials Engineering and Performance, 2018, 27: 1642−1653.

[31] CHANG S, LIN H, TSAO L, HUANG W T, HUANG Y T. Effect of voltage on microstructure and corrosion resistance of microarc oxidation coatings on CP-Ti [J]. Corrosion Engineering, Science and Technology, 2014, 49: 17−22.

[32] GUAN Shi-wei, QI Min, LI Ya-da, WANG Wei-qiang. Morphology evolution of the porous coatings on Ti–xAl alloys by Al adding into Ti during micro-arc oxidation in $Na_2B_4O_7$ electrolyte [J]. Surface & Coatings Technology, 2020, 395: 125948.

[33] VENKATESWARLU K, RAMESHBABU N, SREEKANTH D, BOSE A C, MUTHUPANDI V, SUBRAMANIAN S. Fabrication and characterization of micro-arc oxidized fluoride containing titania films on Cp Ti [J]. Ceramics International, 2013, 39: 801−812.

[34] SANTOS P B, BALDIN E K, KRIEGER D A, CASTRO V V, AGUZZOLI C, FONSECA J C, RODRIGUES M, LOPES M A, MALFATTI C F. Wear performance and osteogenic differentiation behavior of plasma electrolytic oxidation coatings on Ti−6Al−4V alloys: Potential application for bone tissue repairs [J]. Surface & Coatings Technology, 2021, 417: 127179.

[35] ZUO You, LI Tian-lu, YU Pei-hang, ZHAO Zi-cong, CHEN Xiao-yi, ZHANG You, CHEN Fei. Effect of graphene oxide additive on tribocorrosion behavior of MAO coatings prepared on Ti6Al4V alloy [J]. Applied Surface Science, 2019, 480: 26−34.

[36] SHOKOUHFAR M, ALLAHKARAM S R. Effect of incorporation of nanoparticles with different composition on wear and corrosion behavior of ceramic coatings developed on pure titanium by micro arc oxidation [J]. Surface & Coatings Technology, 2017, 309: 767−778.

[37] LUO Si-si, WANG Qun, YE Ren-feng, RAMACHANDRAN C S. Effects of electrolyte concentration on the microstructure and properties of plasma electrolytic oxidation coatings on Ti−6Al−4V alloy [J]. Surface & Coatings Technology, 2019, 375: 864−876.

[38] YAO Zhong-ping, LIU Yun-fu, XU Yong-jun, JIANG Zhao-hua, WANG Fu-ping. Effects of cathode pulse at high frequency on structure and composition of Al_2TiO_5 ceramic coatings on Ti alloy by plasma electrolytic oxidation [J]. Materials Chemistry and Physics, 2011, 126: 227−231.

[39] YEROKHIN A L, NIE X, LEYLAND A, MATTHEWS A.

Characterisation of oxide films produced by plasma electrolytic oxidation of a Ti−6Al−4V alloy [J]. Surface & Coatings Technology, 2000, 130: 195−206.

[40] ADDEPALLI S. Annealing temperature influenced physical properties of Al_2TiO_5 thin films for MIS devices [J]. Advanced Materials Proceedings, 2017, 2: 189−193.

[41] AZARNIYA A, ZEKAVAT M, SOLTANINEJAD M, BAKHSHANDEH F, HOSSEINI H R M, KASHANI S, AMUTHA C, SADRNEZHAAD S K, RAMAKRISHNA S. Preparation of nitrogen-doped aluminium titanate (Al_2TiO_5) nanostructures: Application to removal of organic pollutants from aqueous media [J]. Advanced Powder Technology, 2020, 31: 3328−3341.

[42] GRUNTHANER F J, GRUNTHANER P J, VASQUEZ R P, LEWIS B F, MASERJIAN J, MADHUKAR A. Local atomic and electronic structure of oxide/GaAs and SiO_2/Si interfaces using high-resolution XPS [J]. Journal of Vacuum Science and Technology, 1979, 16: 1443−1453.

[43] WANG Shuai-xing, ZHAO Qing, LIU Dao-xin, DU Nan. Microstructure and elevated temperature tribological behavior of TiO_2/Al_2O_3 composite ceramic coating formed by microarc oxidation of Ti6Al4V alloy [J]. Surface & Coatings Technology, 2015, 272: 343−349.

[44] AKTUĞ S L, DURDU S, KUTBAY I, USTA M. Effect of $Na_2SiO_3·5H_2O$ concentration on microstructure and mechanical properties of plasma electrolytic oxide coatings on AZ31 Mg alloy produced by twin roll casting [J]. Ceramics International, 2016, 42: 1246−1253.

[45] LI Hong, SUN Ye-zi, ZHANG Jin. Effect of ZrO_2 particle on the performance of micro-arc oxidation coatings on Ti6Al4V [J]. Applied Surface Science, 2015, 342: 183−190.

[46] CUI Xue-jun, NING Chuang-ming, SONG Shi-jie, WANG Lin, YANG Ruo-hao. Porosity evaluation of micro-arc oxidation coating through Image-J and electrochemical methods [J]. The Chinese Journal of Nonferrous Metals, 2020, 30: 1101−1109. (in Chinese)

电解液成分对等离子体电解氧化 TC4 合金腐蚀行为和摩擦学性能的影响

杨翠萍[1]，孟宪泽[1]，李鑫冉[1]，李哲轩[1]，严豪杰[1]，伍廉奎[1]，曹发和[1,2]

1. 中山大学 材料学院，深圳 518107；
2. 南方海洋科学与工程广东省实验室(珠海)，珠海 519082

摘　要：在 TC4 合金表面制备 4 种典型等离子体电解氧化(PEO)涂层，研究电解质组成对 PEO 涂层腐蚀行为和摩擦学性能的影响。结果表明，PEO 涂层的腐蚀行为和摩擦学性能与电解质成分密切相关。在含 NaH_2PO_2 的电解液中制备的 PEO 涂层由于内氧化膜较致密而具有最好的耐蚀性能，而在含 $NaAlO_2$ 的电解液中制备的 PEO 涂层由于含有 Al_2O_3 而具有最好的摩擦学性能。为制备具有良好耐蚀性和耐磨性的 PEO 涂层，以 NaH_2PO_2 和 $NaAlO_2$ 为电解液主要成分制备了复合 PEO 涂层。

关键词：Ti6Al4V 合金；等离子体电解氧化；极化曲线；磨损

(Edited by Bing YANG)